THE ATLAS FORWARD CALORIMETERS

John Rutherfoord
University of Arizona, Tucson, Arizona, USA

ABSTRACT

Forward calorimetry completes the nearly 4π coverage for high p_T hadronic events in the ATLAS detector at the LHC. Both the deployment and the technology of the forward calorimeters (FCal) in ATLAS are novel. The FCal physics goals and performance requirements focus on missing E_T and tagging jets. The placement of the FCal relatively close to the interaction point provides many advantages including nearly seamless calorimetry and natural shielding for the muon system. The liquid argon rod/tube electrode structure for the FCal was invented specifically for applications in high rate environments. Recent electron test beam results of an EM prototype show linearity of response better than 1% with energy and angle, energy resolution with a constant term less than 4% with Gaussian tails, and position resolution of order 1 mm.

1 The Role of Forward Calorimeters

At a high luminosity hadron collider such as the LHC at CERN the particle densities and energies are largest at high $|\eta|$, i.e. near the forward and backward directions. Calorimetry is the only useful detector technology which can survive in this environment. Furthermore many compromises are imposed on the calorimeter design in order to meet all the stringent requirements.

In the ATLAS detector at the LHC [1)] the inner detector coverage extends up to $|\eta|$=2.5, the muon coverage up to $|\eta|$=2.7, and the precision calorimetry for electrons and gammas up to $|\eta|$=2.5. Beyond this the only coverage is calorimetric and extends to $|\eta|$=4.9. In this region ATLAS focuses on jets. The ATLAS forward calorimeters cover the region $3.1 < |\eta| < 4.9$.

A major objective of forward calorimetry is physics with missing E_T. Events with high p_T neutrinos or other weakly interacting particles will escape detection but their presence can be inferred by observing events with large momentum imbalance in the transverse direction. Such events can be quite interesting. A major background comes from ordinary events where a jet escapes detection, often down the beam hole. Forward calorimeters close as much of this beam hole as is practical thereby completing the hermetic calorimeter system. Benchmark processes which have guided our performance goals include heavy (500 to 800 GeV) Higgs production with subsequent decay to Z pairs with one Z decaying to charged leptons (electrons or muons) and the other decaying to unobserved neutrinos. The search for Supersymmetry (SUSY) will have pushed the gluino mass limit to 300 GeV at LHC turn-on so missing E_T greater than 100 GeV will set the scale. Sensitive to the missing E_T resolution (dominated by calorimetric coverage) is the decay $A/H \rightarrow \tau^+\tau^-$.

Longitudinal WW, WZ, and ZZ scattering processes leave two recoil jets near the forward and backward directions which can be used as tags to enhance the signal over background. If the Higgs is heavy such processes will act as probes of a poorly understood, strongly interacting, electroweak sector. Many of these tagging jets will fall in the forward calorimeters and it will be a challenge to pick up these above the pileup noise.

2 Performance Requirements

The forward calorimeters primarily detect jets, either tagging jets or jets which would otherwise escape detection and lead to false E_T signatures. This sets the segmentation of the readout to be of order $\Delta\eta \times \Delta\phi = 0.2 \times 0.2$.

We set the E_T resolution to be $\delta E_T/E_T < 10\%$ for $E_T > 100$ GeV. This requires the FCal energy resolution to be $\delta E/E < 7\%$ and and the jet angle resolution to be $\delta\theta/\theta < 7\%$ typically. At the highest $|\eta|$ it is the angle resolution which dominates.

Physics pileup, measured in terms of E_T, is about the same as at lower $|\eta|$. In order to minimize this pileup fast response, of order a beam crossing interval of 25 ns, is required.

The forward calorimeters must be especially radiation hard to insure long-term stability. To set the scale, at every 25 ns beam crossing 7 TeV of energy is deposited in each FCal [2]. The ionization dose varies throughout the FCal from a low of about 10 kRad to values approaching 1 GRad per LHC year. And the flux of neutrons with kinetic energies above 100 keV ranges from 10^4 to 10^6 kHz/cm^2.

3 *INTEGRATING* the FCal into ATLAS

The severe environment near the beam line, dominated by products of collisions at the interaction point (IP), suggests locating the forward calorimeters as far from the IP as possible. This reduces the particle densities and therefore the radiation damage. The original ATLAS design placed the FCal at about 15 m from the IP. But further study [3, 4, 5, 6] showed that there were many advantages to locating the FCal at roughly the same place as the endcap calorimeters, i.e. *integrated* into the endcap. The distance of the ATLAS FCal from the IP is now about 5 m where the density of particles is approximately 9 times greater. Despite the punishment in radiation damage there are many advantages to this design strategy [7].

The calorimetry system is now manifestly *hermetic*. A deep calorimeter system continuously surrounds the IP (with non-projective gaps to route signals and services for the inner detector). A key feature is that *transitions* are minimized. The edges of transitions can be problematic in that hadronic showers near the edges can spray into remote calorimeters with no hint that the energy did not come from the IP. This leads to false reconstruction of the energy flow. The endcap-forward transition in ATLAS now suffers little of this effect.

ATLAS has an *open* muon system, i.e. the muon chambers are not embedded between magnetized iron slabs which would provide natural shielding. So the ATLAS muon chambers are fully exposed to backgrounds (particularly neutrals) in the collision hall. In the early far forward FCal design ATLAS had deployed massive shielding in order to reduce the backgrounds to manageable levels. The newer *integrated* design allows for much more flexibility in optimizing the muon shielding [8, 9] yielding important reductions in the background rates.

With a far forward calorimeter ATLAS was required to leave a clear space from the IP to the FCal so as not to obstruct the particles. This clear space, the need to deploy massive shielding, the desire by the muon people to cover to as high values of $|\eta|$ as possible, and the beam line appurtenances were all in conflict. The space was oversubscribed. The *integrated* design greatly ameliorated this conflict.

There is unavoidable material upstream of all the ATLAS calorimeters. This material is particularly troublesome near the beam line in front of the FCal. Examples include the beam pipe itself which is crossed as shallow angles by the particles but in addition includes flanges, valves, vacuum pumps, vacuum backout appliances, support structures, and, in the case of ATLAS, cryostat walls. With the *integrated* FCal there is less of this material but, more importantly, the *lever arm* from the material to the FCal is much smaller. For particles which shower in the upstream material, that shower cannot spread much over the short distance to the FCal so the energy flow is well collimated along the original direction. For a far

forward calorimeter, on the other hand, the far upstream material causes the energy to spread over so large an area of the FCal that much of it is lost in the pileup.

Finally the smaller physical size of the *integrated* FCal leads to a savings, some of which can be used for a higher quality device.

4 The Liquid Argon Technology

The ATLAS FCal is a liquid argon, ionization, sampling calorimeter. Because liquid argon and the absorber metals are radiation hard it is anticipated that the FCal performance will be stable over the life of the detector. Care will be required in selecting the several additional materials (e.g. readout cables) which go into the construction in order to ensure they also will not degrade with the expected exposure. The choice of liquid argon is natural because the FCal lies within the ATLAS Hadronic Endcap Calorimeter (HEC) which is a liquid argon parallel plate design. Along with the EM endcap 'Spanish Fan', the HEC and FCal will all sit within the same cryostat.

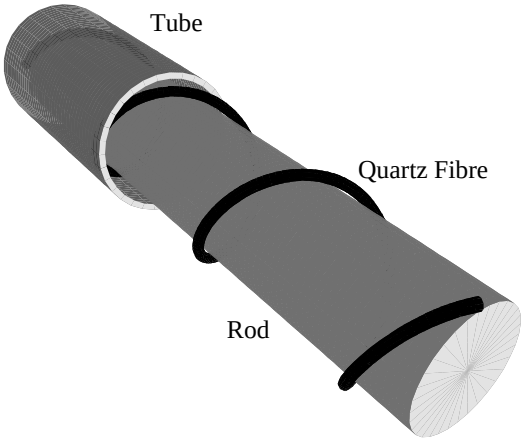

Figure 1: Tube electrode with the inner rod pulled out to expose the spiraled quartz fiber holding the rod coaxially within the tube. Liquid argon fills this gap between rod and tube which, for the EM module, is 250 μm across. The rod is held at positive high voltage while the tube is grounded.

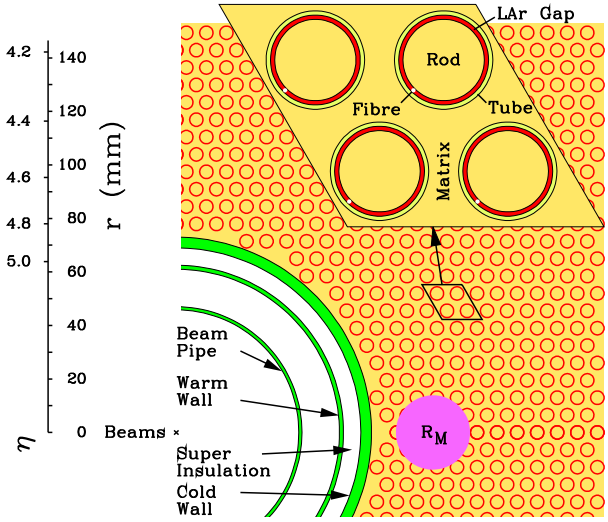

Figure 2: Front face of the EM forward calorimeter module in the region of the beam pipe. The circle labelled R_M indicates the Molière radius for e.m. showers. The insert at the upper right shows the detail of four tube electrodes embedded in the absorber matrix. On the left is a scale in mm and η.

But the ATLAS FCal is not a conventional liquid argon calorimeter. The liquid argon gap in the EM FCal module is chosen to be 250 μm to avoid the ion

buildup problem [10] resulting from the low mobility of the positive charge carriers in the argon. At sufficiently high ionization rates (due to pileup events) a threshold is reached above which the electric field distortion significantly degrades the electron signal. Smaller gaps allow the FCal to stay below this threshold. The smaller gaps also lead to a much faster signal. The triangular current pulse at the electrode has a full drift time of 50 ns as opposed to the 400 ns of more conventional 2 mm gaps in many liquid argon sampling calorimeters. After 25 ns 75% of the signal has already accumulated on the electrode. The readout and electronics shape this current pulse to a peaking time of about 40 ns. This leads to an *rms* pileup noise which is about 30% larger than the irreducible pileup from an ideal detector which has an integration time of one bunch crossing. We say the actual pulse leads to a pileup penalty of a factor 1.3.

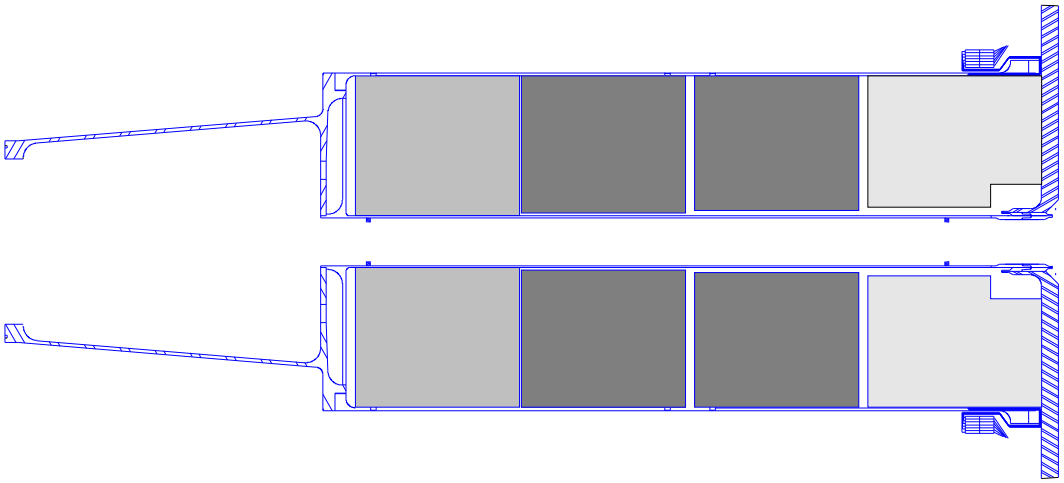

Figure 3: Slice along the beamline of the FCal modules housed in their support tube. The EM module in medium gray is on the left, followed by the two hadronic modules in dark gray. The light gray module at the right is the copper 'plug' which provides extra shielding for the muon system.

Precision small gaps are difficult to maintain in a parallel plate design so we have chosen an electrode structure based on tubes and rods as shown in Figure 1. The gap between the inner solid rod and the outer tube is maintained by a spiraled quartz fiber of 250 μm diameter. Liquid argon, the ionizing (sensitive) medium, fills the rest of the gap not occupied by the fiber (98.7% of the volume of the gap). The current of electrons drifting toward the rod constitutes the signal. Note that the figure is an *exploded* view, i.e. the rod has been pulled out to expose the fiber. The rod and tube are made of the same material as the absorber matrix in which these electrodes are embedded in a hexagonal array as shown in Figure 2.

The rods, tubes, and absorber matrix of the EM modules are made of

copper. Copper was chosen because the Molière radius (14 mm) is not too small (in contrast to Tungsten). This makes the response across the front face of the module reasonably uniform [11]. The rods and matrix in the two (at each end) hadronic modules are Tungsten. The liquid argon gap in the first hadronic module is 375 μm while that in the second is 500 μm. These larger gaps deeper in the calorimeter are allowed because the ionization density from showers is lower here than in the EM module. All modules are 450 mm in depth with an outer radius of 450 mm. The EM modules are 25 X0 deep or 2.5 λ. The hadronic modules are each 3.4 λ deep for a total active depth of 9.3 λ. Behind the second hadronic module at each end is a 'plug' of passive copper to help shield the muon system. The three modules at one end of ATLAS are shown in their support tube in Figure 3. The nearest-neighbor spacing of electrodes in the EM section is 7.5 mm center-to-center and increases in the hadronic modules so that they are pseudo-projective.

5 Electron Test Beam Results

We have built and tested a prototype of the EM FCal module [12, 13]. The prototype has the full 450 mm depth of the actual device but is only 180 mm in diameter. Four tube electrodes are ganged together at the module to form a readout channel with total capacitance of 1.45 nF. The prototype has 91 such channels. The signals are transferred from the electrodes to the electronics via 20 Ω coax cables with polyimide dielectric and insulation for radiation hardness. The cable in the cryostat is 4.5 m long and 1 m outside the cryostat to simulate the actual cable lengths. The preamps, located outside the cryostat, are the so-called $\emptyset$T type [14, 15]. Modified Sallen-Key (equivalent to CR-RC) shapers give a peaking time for the liquid argon pulses of about 40 ns. Track & Holds convert the peaks of the pulses to voltage levels which are fed to 11-bit FERA ADC's read by CAMAC into a PC and onto a disk co-mounted with a VAXStation. Incoherent noise per channel was under 80 MeV with a coherent noise contribution of about 20% of this. The coherent noise appears to have a coherence length limited to 16 channels. Our preamps, shapers, and Track & Holds were all mounted on motherboards with 16 channels each and cables interconnecting these came in groups of 16. We have not yet isolated the source of the coherent noise but it is not significant for the energies and cluster sizes used in this test.

The high voltage (only 250 V to give 10 kV/cm electric field) is applied near the preamp input (separated by a blocking capacitor on the preamp board) and reaches the electrodes via the readout coax cable. The calibration pulse is also injected at the preamp input. None of the results presented below use the calibration. Those preamps corresponding to channels which are struck by beam

electrons (17 in all) are calibrated by beam and are uniform to better than 0.5% using the same calibration constant for all channels.

Three scintillators form the trigger with the defining size of 5 by 5 cm. The electron beam is defocussed to fill this area uniformly. A veto wall eliminates triggers with additional charged particles outside this area. Ten planes of 1 mm spacing MWPC's (5x and 5y) allows good tracking of the electron. Optional dead material (Aluminum blocks) can be placed upstream of the prototype to simulate the anticipated situation in ATLAS. Rohacell^{TM} displaces liquid argon upstream and downstream of the prototype inside the cryostat. Downstream of the prototype is a crude hadronic tail catcher consisting of iron-scintillator layers. After 10 λ a small scintillator centered on the beam tags muons. An argon purity monitor [16, 17] and oxygen analyzer ensure that contamination is at or below the 0.5 ppm oxygen equivalent level.

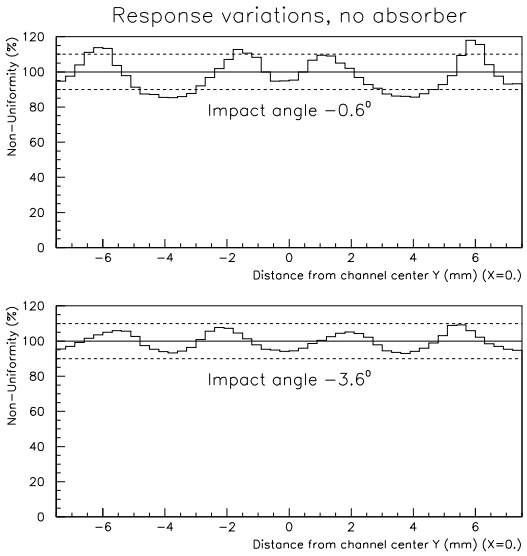

Figure 4: Normalized energy response versus position at two incident electron angles.

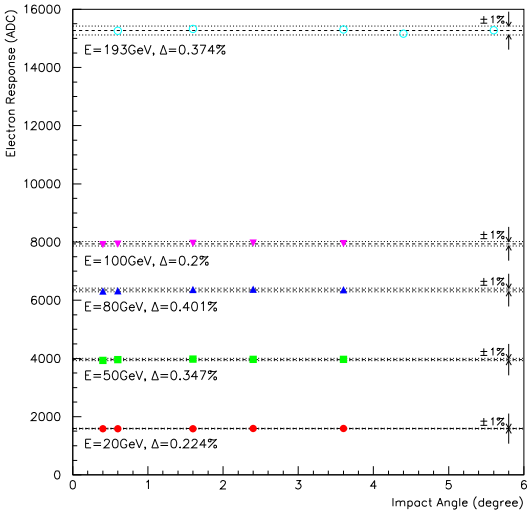

Figure 5: Prototype response to electrons versus angle to the normal for different electron energies.

In the actual FCal particles enter at angles between 0.8° and 4.7° to the normal. Channeling effects are a potential problem as evidenced by a position dependence to the response. Electrons which strike the prototype at small angles to the normal and near the argon gap give a response of order 15% above average while electrons which strike the center of a rod give a response about 15% below average. At larger angles to the normal this position dependence of the response washes out. At a typical angle of 3.6° the peak variation is of order ±8%. For most

of the angular range the *rms* position response variation is under 5% as shown in Figure 4.

Averaging over position the response variation with angle is very uniform, within $\pm 1\%$ full width. Figure 5 shows that all the data points lie within this range over a spread in angles beyond that covered by the FCal.

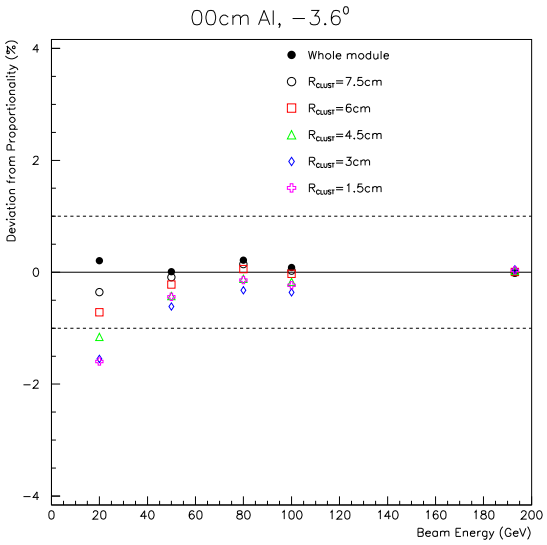

Figure 6: Deviation of the energy response from a straight line constrained to the origin for different clustering radii.

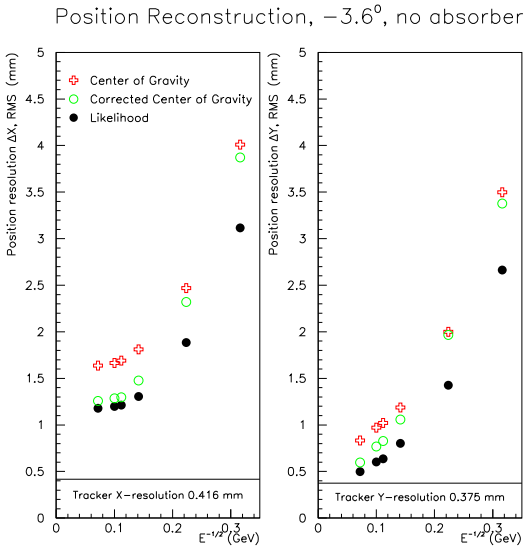

Figure 7: Position resolution versus $1/\sqrt{E}$ using different algorithms.

When analyzing the data we include only those channels within a 'cluster radius' of the center-of-energy. This center is determined by a clustering algorithm (not by the MWPC's). Various cluster radii will be used in the following results. A cluster radius of 35 mm generally contains 95% of the energy (at 3.6°) except at our lowest energy point at 20 GeV where the 95% containment radius jumps to 40 mm.

Figure 6 shows the deviation from a straight line (constrained to the origin) of the energy response of the prototype EM module for different clustering radii. For large radii the linearity is well under $\pm 0.5\%$. Smaller clustering radii show the small but discernible energy dependence of the transverse shower size confirming that lower energy electromagnetic showers spread a bit more.

The fine readout channel granularity allows a good position determination from shower sharing. Three reconstruction techniques have been used. When compared to the position determined from the MWPC's an *rms* position resolution can be determined. These data are shown in Figure 7 versus $1/\sqrt{E}$. The beam lies in

the x-z plane making an angle of 3.6° to the z axis. Longitudinal shower fluctuations couple into the position determination in this plane so the position resolution is worse than in the y-z plane where the beam angle is normal to the prototype. The MWPC resolution (which is not subtracted in this analysis) limits the determination of the position resolution to about 0.4 mm. The excellent position resolution seen here allows us to remove most of the position dependence of the response from the test beam data. We will show this below.

The *rms* percent energy resolution for electrons is plotted versus cluster radius for different electron beam energies in Figure 8. Correcting for the variation of response due to position improves the energy resolution substantially at the higher energies. Note that at the lower energies the electronics noise is not negligible for larger cluster radii.

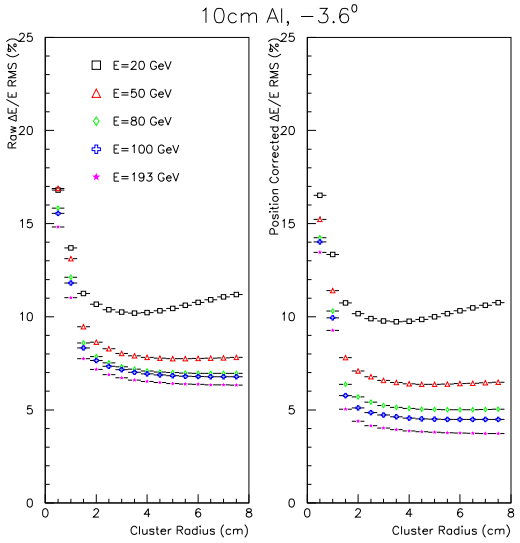

Figure 8: Percent energy resolution versus cluster radius for different electron beam energies without and with position correction.

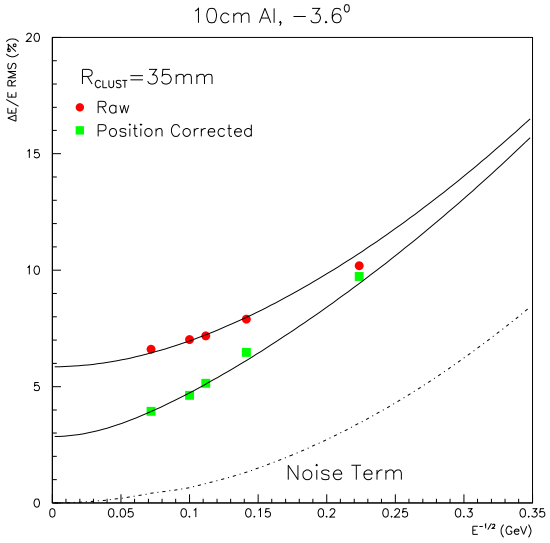

Figure 9: Percent energy resolution for electrons versus $1/\sqrt{E}$ for fixed cluster radius of 35 mm without and with position correction.

Choosing a cluster radius of 35 mm we have plotted in Figure 9 the *rms* percent energy resolution versus $1/\sqrt{E}$ without and with a correction for response variations due to position. A fit to this data of the form $\Delta E/E = a \oplus b/\sqrt{E} \oplus c/E$ yields the usual summary energy resolution terms. The so-called constant term is a, while the stochastic term is b, and the noise term (in this case due only to electronics) is c. The noise term for a cluster radius of 35 mm is plotted at the bottom of the figure. Repeating this fit for different cluster radii yields the data of Figure 10. Note

that the response variation due to position contributes to the constant term.

As noted earlier the FCal measures jets. The EM module, a prototype of which we have exposed to the testbeam, measures the EM components of such jets and the early parts of the hadronic components. Jets typically contain several EM components spread over the front face of the FCal into an area large compared to a unit cell. (A unit cell contains one tube electrode.) So the response variations due to position are averaged over. To evaluate the effect of this averaging we have taken tagging jets generated via Pythia for the process $pp \rightarrow HX \rightarrow ZZjjX$. We then decayed each Z into neutrinos to avoid dealing with the decay products. We next picked out the EM components of each tagging jet and, using our testbeam data as a lookup table, simulated the response of the FCal. The results, shown in Figure 11, yield a constant term of about 3%, approximately what we determined after position correction of the electron data as seen in Figure 10.

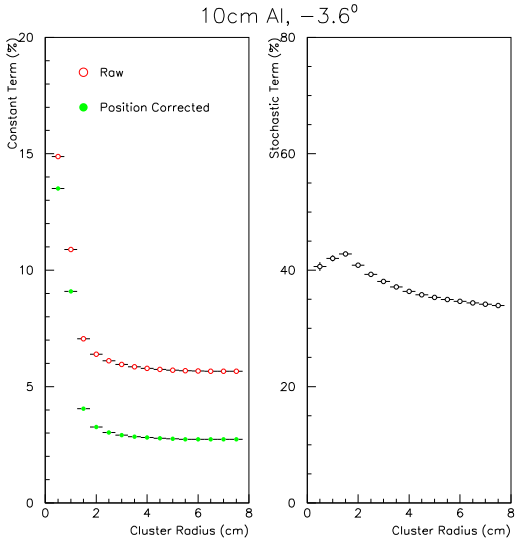

Figure 10: Constant term and stochastic term in the energy resolution parameterization versus cluster radius without and with position correction.

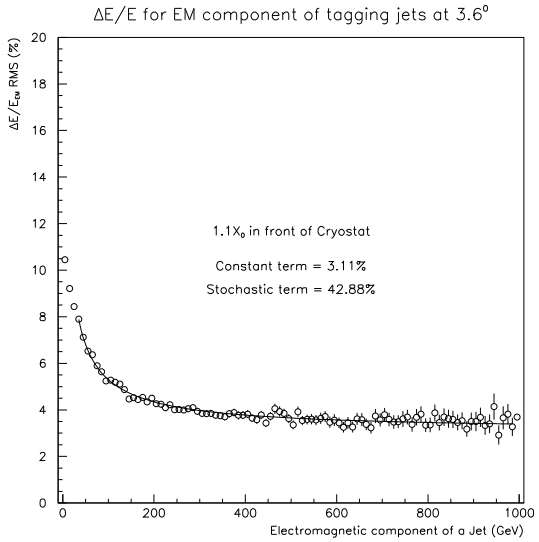

Figure 11: Calculated percent energy resolution for the electromagnetic component of tagging jets from 800 GeV Higgs production versus the energy of that electromagnetic component.

Up to this point we have concentrated on the prototype performance at a typical angle of incidence to the normal of 3.6°. Figure 12 shows how the energy resolution varies with incident angle after the correction for the response variation due to position. While the energy response is quite constant with angle (see Figure 5) the *rms* energy resolution improves with angle as is shown in Figure 12. At the

smallest angles relevant to the FCal, of order 1°, the angle resolution dominates the E_T determination so the energy resolution, if under control, is not the critical parameter. Figure 12 shows that the energy resolution for EM energy deposits is well within our requirements.

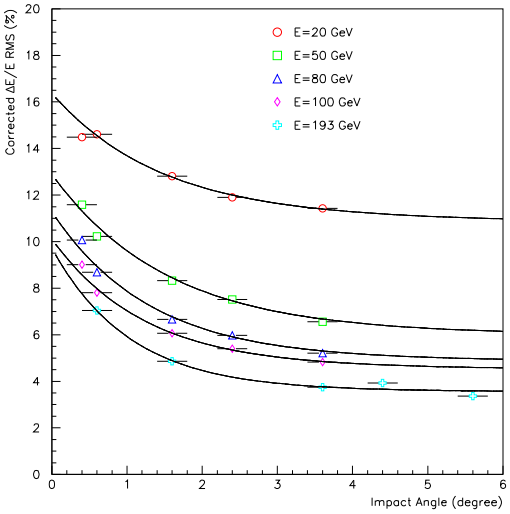

Figure 12: Percent energy resolution versus angle for different electron beam energies with position correction.

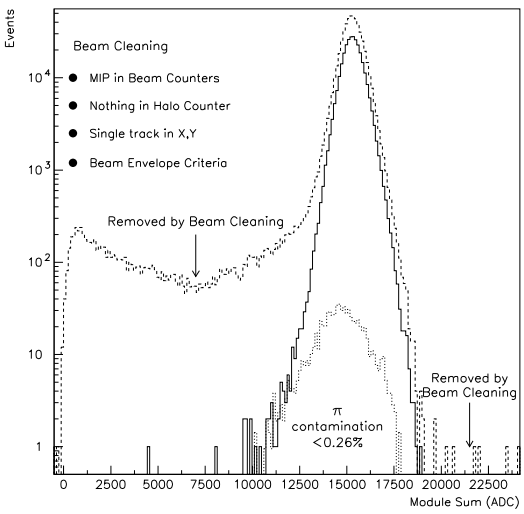

Figure 13: Electron energy resolution function without beam cleaning (dashed), with beam cleaning (solid), and pion contamination (dotted) for 193 GeV beam at 3.6°.

Tails on the energy resolution function can be a problem. Figure 13 shows the energy resolution function for 193 GeV electrons over almost five orders of magnitude. With only simple cuts to eliminate pions there is a large tail on the low energy side (approximately 1% of the peak height) and a few events on the high side outside the peak. After examination of single events we could see rare instances of a low energy cluster centered on the MWPC track projection but another neutral cluster elsewhere in the prototype. This was clear evidence for electron bremsstrahlung upstream in the beam line. The events with low pulse height occur when the bremsstrahlung photon misses the prototype. A severe cut on the beam angle appears to eliminate all such events with a concomitant loss of about 50% of the good events. The cut has the virtue that it is completely unbiased. An estimate of the pion contamination surviving the cuts, obtained from separate pion runs, appears to explain the remaining low energy tail well below the 10^{-4} level.

6 Summary

ATLAS has elected an unconventional location for its forward calorimeters resulting in many benefits. The chosen technology employs a novel liquid argon electrode structure. Test beam results with electrons show performance exceeding the requirements.

References

1. The ATLAS collaboration, *Technical Proposal for a General-Purpose pp Experiment at the Large Hadron Collider at CERN*, CERN/LHCC/94-43 (1994).

2. J. Rutherfoord, *Heating and Cooling a Forward Calorimeter*, ATLAS Internal Note CAL-NO-056, 21 June 1994.

3. J. Rutherfoord, L. Shaver, and M. Shupe, *The ATLAS Forward Region*, ATLAS Internal Note CAL-NO-035, 1994.

4. M. Shupe and J. Rutherfoord, *Three Options for the ATLAS Forward Region: Particle and Jet Response and Fluence Results from a GEANT Mixture Description of the Detector*, ATLAS Internal Note CAL-NO-036, 1994; M.Shupe, *Using GEANT Mixtures for the Precise Simulation of Particle and Jet Response, and Particle Fluxes in ATLAS*, ATLAS Internal Note CAL-NO-037, 1994.

5. J. Rutherfoord, A. Savin, L. Shaver, M. Shupe, *The ATLAS Integrated Forward Calorimeter, Progress on Answers to Calorimetry Panel Questions*, ATLAS Internal Note CAL-NO-055, 27 May 1994.

6. Laurie Waters and William B. Wilson, *LAHET/MCNP/CINDER'90 Activation Calculations for the ATLAS Integrated Forward Calorimeter Concept*, ATLAS Internal Note CAL-NO-047, 19 July 1994.

7. J. Dowell *et al.*, *Report of the ATLAS Review Panel on Forward Calorimetry*, ATLAS Internal Note GEN-NO-007, 26 August 1994.

8. M. Shupe, *ATLAS Muon Region Background Fluxes in Four Forward Configurations*, ATLAS Internal Note GEN-NO-011, 7 November 1994.

9. G .Battistoni, A. Ferrari, and P.R. Sala, *Background calculations for the ATLAS detector and hall*, ATLAS Internal Note, GEN-NO-010, 13 October 1994.

10. J. Rutherfoord, *Ion Loading in Liquid Ionization Calorimeters*, GEM TN-91-27, 25 October 1991; J.Rutherfoord, *Testing for Effects of Ion Loading in Liquid Ionization Calorimeters*, GEM TN-93-410, 18 May 1993.

11. P. Loch, *Tube Radius Optimization for the Electromagnetic Forward Calorimeter in ATLAS*, ATLAS Internal Note LARG-NO-039, 12 April 1996.

12. ATLAS members contributing to the test beam run reported here are J.C. Armitage (Carleton University, Ottawa), A. Artamonov, V. Epchtein, V. Jemanov, V. Khovansky, M. Ryabinin, P. Shatalov (ITEP, Moscow), L. Austin, K. Johns, P. Loch, R. Norton, J. Rutherfoord, A. Savin, L. Shaver, M. Shupe, J. Steinberg, D. Tompkins (University of Arizona), J.K. Mayer, R.S. Orr, and G. Stairs (University of Toronto).

13. Earlier test beam results are reported in M.I. Ferguson *et al.*, *Electron Testbeam Results for the ATLAS Liquid Argon Forward Calorimeter Prototype*, accepted for publication in Nucl. Instrum. and Methods **A**, July 1996; A. Savin, *Beam Test of Liquid Argon Tube Calorimeter Prototype*, Proc. of the 5$^{\text{th}}$ Int. Conf. on Calorimetry in High Energy Physics, Brookhaven, New York Sept 25 – Oct 1, 1994, ed. Howard A. Gordon and Doris Rueger, World Scientific 1995; M.I. Ferguson *et al.*, *A liquid argon forward calorimeter prototype: beam test results*, ATLAS Internal Note CAL-NO-042, 18 January 1994.

14. R.L. Chase, C. de La Taille, S. Rescia, and N. Seguin-Moreau, *Transmission lines connection between detector and front end electronics in liquid argon calorimetry*, Nucl. Instr. and Meth. **A330** (1993) 228-242; R.L. Chase, C. de La Taille, and N. Seguin-Moreau, *Experimental results on cable-coupled preamplifiers ($\emptyset T$)*, Nucl. Instr. and Meth. **A343** (1994) 598-605.

15. J. Rutherfoord, *The Electronics Choice for the ATLAS FCal*, ATLAS Internal Note CAL-NO-087, 6 November 1995.

16. G.C. Blazey, *Monitoring Liquid Argon Purity at DZero*, in Proc of Int. Conf. on Calorimetry in High Energy Physics, Batavia, IL Oct. 29 – Nov. 1, 1990 (1991).

17. A. Attard, J.K. Mayer, R.S. Orr, G.S. Stairs, and J.C. Armitage, *Development of a Portable Liquid Argon Purity Monitor System*, ATLAS Internal Note LARG-NO-032, 15 December 1995.